A New Sea Ice Model for GME

Dmitrii Mironov and Bodo Ritter
Deutscher Wetterdienst, Offenbach am Main, Germany
(dmitrii.mironov@dwd.de, bodo.ritter@dwd.de)

Abstract

A bulk thermodynamic ice model for use in numerical weather prediction (NWP) is developed. The model is based on a self-similar parametric representation (assumed shape) of the evolving temperature profile within the ice and on the integral heat budget of the ice slab. The model solves two ordinary differential equations for the two time-dependent quantities, the ice surface temperature and the ice thickness. The horizontal distribution of the ice cover is governed by the data assimilation scheme. The proposed ice model is implemented into the global NWP system GME of the German Weather Service. In the present operational configuration, no fractional ice cover in the GME grid box and no snow over the ice are considered (although provision is made to account for the snow layer, using the bulk model framework). Results from numerical experiments show a satisfactory agreement with available observational data on the two-metre temperature in the Arctic. Numerical results show little sensitivity to the details of the ice model itself. This justifies the use of a simplified bulk approach to model the ice thermodynamics in NWP. As compared to the finite-difference heat-transfer approach, the bulk approach allows to save computational resources without a detectable loss in accuracy. Sensitivity tests indicate that the ice surface temperature is sensitive to cloud cover as it controls the radiation energy budget, particularly during winter, and to ice albedo with respect to solar radiation, particularly during summer. In GME, the ice albedo is related to ice surface temperature through an empirical formulation. That formulation is meant to implicitly account, in a rather approximate way, for the seasonal changes of the ice albedo. Further efforts should go into the development of a refined formulation for the ice albedo. The fractional ice cover and the snow layer over the ice may also need to be considered.

1 Introduction

In this note, we describe the new operational sea ice model for the numerical weather prediction (NWP) system GME (Majewski et al. 2002) of the German Weather Service (DWD). We recall that an old GME ice model is actually a parameterization rule that simply sets the ice surface temperature to a climatologically mean value and keeps it constant over the forecast period. The new model accounts for thermodynamic processes only, i.e. no ice rheology is considered. The reader is referred to `http://stommel.tamu.edu/~baum/ocean_models.html`, where detailed descriptions of several dynamic-thermodynamic ice models and further references can be found. As for the ice thermodynamics, the model presented here is broadly similar to most other models developed to date (summaries are given by Leppäranta 1993, and Launiainen and Cheng 1998). A distinguishing feature of the model is the treatment of the heat transfer through the ice. Most currently used ice models carry the heat transfer equation that is solved on a finite difference grid where the number of grid points and the grid spacing differ with the application. We use the integral, or bulk, approach.

The approach taken here is based on a self-similar parametric representation (assumed shape) of the evolving temperature profile within the ice that is conceptually similar to a parametric representation of the temperature profile in the seasonal thermocline in the ocean or lakes. The idea was put forward by Kitaigorodskii and Miropolsky (1970) to describe the vertical temperature structure of the oceanic seasonal thermocline. The essence of the concept (see an overview in Mironov 2004) is that the dimensionless temperature profile in the thermocline can be fairly accurately parameterised through a "universal" function of dimensionless depth, where the temperature difference across the thermocline and its thickness are used as the relevant scaling parameters.[1] The idea has found extensive use in environmental modelling. A number of computationally efficient models based on a self-similar representation of the temperature profile have been developed and successfully applied to simulate the evolution of the mixed layer and seasonal thermocline in the ocean (e.g. Kitaigorodskii and Miropolsky 1970, Kamenkovich and Kharkov 1975, Arsenyev and Felzenbaum 1977, Filyushkin and Miropolsky 1981), the atmospheric convectively mixed layer capped by a temperature inversion (e.g. Deardorff 1979, Fedorovich and Mironov 1995), and the seasonal cycle of temperature and mixing in fresh-water lakes (e.g. Zilitinkevich 1991, Mironov et al. 1991, Zilitinkevich et al. 1992). Here we use the idea of self-similarity to parameterize the temperature profile within the ice.

The ice model is developed in section 2, and the implementation into the NWP system GME of DWD is discussed in section 3. As a first step, a simplified version of the proposed model is implemented into GME, where the snow layer over the ice and the heat flux from water to ice are neglected, and the volumetric character of the solar radiation heating is ignored (i.e. the solar radiation flux does not appear as a source term in the heat transfer equation but enters the problem through the boundary condition at the air-ice interface). The model outlined in section 2 is an extended version, where the above features are accounted for. Both the ice layer and the snow layer are modelled using the same basic concept, that is a parametric representation (assumed shape) of the evolving temperature profile. In section 4, results from numerical experiments with GME are discussed and compared with available empirical data and with the output from the ECMWF global NWP system (Integrated Forecasting System – IFS). Conclusions are presented in section 5.

2 Model Formulation

The equations of the ice-snow model are derived from the heat transfer equation

$$\frac{\partial}{\partial t}\rho c\theta = -\frac{\partial}{\partial z}(Q+I) + f_M(z)L_f\frac{dM}{dt}. \tag{1}$$

Here, t is time, z is the vertical co-ordinate (positive upward) with the origin at the ice-water interface, ρ is the density of the medium in question (snow or ice), c its specific heat, θ is the temperature, I is the solar radiation flux, Q is the vertical heat flux (the long-wave radiation fluxes are assumed to enter through the boundary condition at the lower boundary of the atmosphere), M is the mass of snow or ice per unit area, and L_f is the latent heat of fusion. The last term on the r.h.s. of Eq. (1) is the source term that describes the rate of heat release/consumption due to accretion/melting of snow and ice. The function $f_M(z)$ satisfies the normalization conditions

$$\int_{H_i}^{H_i+H_s} f_M(z)dz = 1, \qquad \int_0^{H_i} f_M(z)dz = 1, \tag{2}$$

where H_i is the ice thickness, and H_s is the thickness of snow overlaying the ice.

The ice-snow model presented below includes a number of thermodynamic parameters. These are taken to be constant except for the snow density and the snow heat conductivity that are functions of snow depth and snow age and are, therefore, time-dependent.

[1] Notice a close analogy between the concept of self-similarity of the thermocline and the concept of the mixed layer that has been successfully used in geophysical fluid dynamics over several decades. Indeed, using the mixed-layer temperature $\theta_m(t)$ and its depth $h_m(t)$ as appropriate scales, the mixed-layer concept states that the dimensionless temperature profile can be expressed through a universal function of dimensionless depth, where that universal function is simply a constant equal to one, $\theta(z,t)/\theta_m(t) = \Phi_m(\zeta) \equiv 1$, $\zeta = z/h_m(t)$. A function that describes the temperature profile in the thermocline is not merely a constant but a more sophisticated function of dimensionless depth.

2.1 Parameterization of the Temperature Profile

We adopt the following parametric representation of the evolving temperature profile within ice and snow:

$$\theta(z,t) = \begin{cases} \theta_f + [\theta_i(t) - \theta_f]\Phi_i(\zeta_i) & \text{at} \quad 0 \le z \le H_i(t) \\ \theta_i(t) + [\theta_s(t) - \theta_i(t)]\Phi_s(\zeta_s) & \text{at} \quad H_i(t) \le z \le H_i(t) + H_s(t). \end{cases} \tag{3}$$

Here, θ_f is the freezing point at the underside of the ice, θ_i is the temperature at the snow-ice interface, and θ_s is the temperature at the air-snow interface. The freezing point θ_f is a decreasing function of salinity that is equal to the fresh-water freezing point θ_{f0} when the salinity is zero. Dimensionless universal functions $\Phi_i \equiv [\theta(z,t) - \theta_f]/[\theta_i(t) - \theta_f]$ and $\Phi_s \equiv [\theta(z,t) - \theta_i(t)]/[\theta_s(t) - \theta_i(t)]$ of dimensionless heights $\zeta_i \equiv z/H_i(t)$ and $\zeta_s \equiv [z - H_i(t)]/H_s(t)$, respectively, satisfy the boundary conditions $\Phi_i(0) = 0$, $\Phi_i(1) = 1$, $\Phi_s(0) = 0$ and $\Phi_s(1) = 1$. In what follows, the arguments of functions dependent on time and height are not indicated, unless it is indispensable.

According to Eq. (3), the heat fluxes through ice, Q_i, and through snow, Q_s, due to molecular heat conduction are given by

$$Q_i = -\kappa_i \frac{\theta_i - \theta_f}{H_i}\frac{d\Phi_i}{d\zeta_i}, \qquad Q_s = -\kappa_s \frac{\theta_s - \theta_i}{H_s}\frac{d\Phi_s}{d\zeta_s}, \tag{4}$$

where κ_i and κ_s are the heat conductivities of ice and snow, respectively.

2.2 Heat Budget

The parameterization of the temperature profile (3) should satisfy the heat transfer equation (1). Consider first the regime where no melting at the snow surface (ice surface, when snow is absent) takes place. In this regime, the heat flux Q is continuous at $z = H_i + H_s$, whereas it may undergo a zero-order jump at the ice-water interface where the ice ablation/accretion takes place. Then, the normalization function f_M is equal to zero throughout the snow-ice cover except at the ice-water interface where $f_M = \delta(0)$, $\delta(z)$ being the Dirac delta function. Integrating Eq. (1) over z from just above the ice-water interface $z = +0$ to the air-snow interface $z = H_i + H_s$ with due regard for the parameterization of the temperature profile (3), we obtain the equation of the heat budget of the snow-ice cover,

$$\frac{d}{dt}\{\rho_i c_i H_i [\theta_f + C_{*i}(\theta_i - \theta_f)] + \rho_s c_s H_s [\theta_i + C_{*s}(\theta_s - \theta_i)]\} - \rho_s c_s \theta_s \frac{d}{dt}(H_i + H_s) =$$

$$-(Q_a + I_a) + I(0) - \Phi_i'(0)\kappa_i \frac{\theta_i - \theta_f}{H_i}. \tag{5}$$

Here, ρ_i and ρ_s are the densities of ice and of snow, respectively; c_i and c_s are specific heats of these media; I_a is the solar radiation flux at the air-snow or, if snow is absent, at the air-ice interface; and Q_a is the heat flux in the air layer adjacent to the snow (ice) surface. Hereafter, a prime denotes a derivative of the shape function Φ_i/Φ_s with respect to the dimensionless height ζ_i/ζ_s. The radiation heat flux I_a that penetrates into the interior of the snow-ice cover is the surface value of the incident solar radiation flux from the atmosphere multiplied by $1 - \alpha$, α being the surface albedo of snow or ice with respect to solar radiation. The heat flux Q_a is a sum of the sensible and latent heat fluxes and the long-wave radiation fluxes at the air-snow (air-ice) interface. It is a rather sophisticated function of the surface air layer parameters, of cloudiness and of the temperature at the air-snow (air-ice) interface. The dimensionless parameters C_{*i} and C_{*s}, the so-called "shape factors", are given by

$$C_{*i} = \int_0^1 \Phi_i(\zeta_i)d\zeta_i, \qquad C_{*s} = \int_0^1 \Phi_s(\zeta_s)d\zeta_s. \tag{6}$$

The heat flux at the snow-ice interface is assumed to be continuous, that is

$$-\kappa_i \frac{\theta_i - \theta_f}{H_i} \Phi_i'(1) = -\kappa_s \frac{\theta_s - \theta_i}{H_s} \Phi_s'(0). \tag{7}$$

Equations (5) and (7) serve to determine temperatures at the air-snow and at the snow-ice interfaces, when no melting at the snow surface (ice surface, when snow is absent) takes place. During the snow (ice) melting from above, the surface temperature remains equal to the freezing point.

2.3 Snow and Ice Thickness

The accumulation of snow is not computed within the ice-snow model. The rate of snow accumulation is assumed to be a known time-dependent quantity that is provided by the atmospheric model or is known from observations. Then, the evolution of the snow thickness during the snow accumulation and no melting is computed from

$$\frac{dH_s}{dt} = \frac{1}{\rho_s} \left(\frac{dM_s}{dt} \right)_a - \frac{H_s}{\rho_s} \frac{d\rho_s}{dt}, \tag{8}$$

where $M_s = \rho_s H_s$ is the snow mass per unit area, and $(dM_s/dt)_a$ is the (given) rate of snow accumulation.

Considering the sea ice, we account for the effect of brine rejection on the ice salinity and hence on the freezing point. However, the effect of internal brine pockets (e.g. Semtner 1976) is neglected. When the temperature θ_i at the upper surface of the ice (θ_i is equal to θ_s if snow is absent) is below the freezing point θ_f, the heat conduction through the ice causes the ice growth. This growth is accompanied by a release of heat at the lower surface of the ice that occurs at a rate $L_f dM_i/dt$, where $M_i = \rho_i H_i$ is the ice mass per unit area. Integrating Eq. (1) over z from $z = -0$ to $z = +0$, where the heat source term due to the ice accretion is $\delta(0) L_f dM_i/dt$, we obtain the equation for the ice thickness. It reads

$$\frac{dH_i}{dt} = -\Phi_i'(0) \frac{\kappa_i}{\rho_i L_f} \frac{\theta_i - \theta_f}{H_i} - \frac{Q_w}{\rho_i L_f}, \tag{9}$$

where Q_w is the heat flux from water to ice. In case the heat flux from water to ice exceeds the heat flux within the ice, ice ablation takes place.

As the atmosphere heats the snow surface, the surface temperature increases and snow melting eventually sets in. Since snow consists of fresh water, melting starts when the surface temperature reaches the fresh-water freezing point θ_{f0}. The snow melting is accompanied by a consumption of heat in the snow layer that occurs at a rate $L_f dM_s/dt = L_f d\rho_s H_s/dt$. Notice that the exact form of the normalization function f_M is not required by virtue of the normalization condition given by the first member of Eq. (2). Integrating Eq. (1) over z from $z = H_i$ to $z = H_i + H_s + 0$ with due regard for the heat loss due to snow melting, then adding the (given) rate of snow accumulation, we obtain

$$\left[1 + (1 - C_{*s}) R_{\theta s} \frac{2 + R_H}{1 + R_H}\right] \frac{dH_s}{dt} + R_{\theta s} \left(1 - \frac{1 - C_{*s}}{1 + R_H} \frac{H_s}{H_i}\right) \frac{dH_i}{dt} =$$

$$\frac{1}{\rho_s L_f} \left[Q_a + I_a - I(H_i) + \Phi_s'(0) \kappa_s \frac{\theta_s - \theta_i}{H_s}\right] +$$

$$+\frac{1}{\rho_s} \left(\frac{dM_s}{dt}\right)_a + R_{\theta s} \frac{1 - C_{*s}}{1 + R_H} \frac{H_s}{\kappa_s} \frac{d\kappa_s}{dt} + \left(\frac{c_s \theta_i}{L_f} - 1 + C_{*s} R_{\theta s}\right) \frac{H_s}{\rho_s} \frac{d\rho_s}{dt}, \tag{10}$$

where $R_{\theta s} = {L_f}^{-1} c_s(\theta_s - \theta_i)$ and $R_H = [\Phi_s'(0)\kappa_s H_i]^{-1} [\Phi_i'(1)\kappa_i H_s]$.

The ice melting is accompanied by a consumption of heat at a rate $L_f dM_i/dt = L_f d\rho_i H_i/dt$. Again, the exact form of the function f_M is not required by virtue of the normalization condition given by the second member of Eq. (2). Integrating Eq. (1) over z from $z = -0$ to $z = H_i$, we obtain

$$\left[1 + R_{\theta i}\left(1 - C_{*i}\frac{1+2R_H}{1+R_H}\right)\right]\frac{dH_i}{dt} + C_{*i}R_{\theta i}\frac{R_H}{1+R_H}\frac{H_i}{H_s}\frac{dH_s}{dt} =$$

$$\frac{1}{\rho_i L_f}\left[-Q_w - I(0) + I(H_i) - \Phi_i'(1)\kappa_i\frac{\theta_i - \theta_f}{H_i}\right] + C_{*i}R_{\theta i}\frac{R_H}{1+R_H}\frac{H_i}{\kappa_s}\frac{d\kappa_s}{dt}, \tag{11}$$

where $R_{\theta i} = {L_f}^{-1} c_i(\theta_i - \theta_f)$.

During the snow-ice melting, the surface temperature remains equal to the fresh-water freezing point, $\theta_s = \theta_{f0}$, and the temperature θ_i is computed from Eq. (7).

Notice finally that ice melting may occur at the lower surface of the ice, even though there is no heating from the water below the ice. Brine rejection from the sea ice leads to its desalinization. This results in a marked salinity gradient across the ice and hence in a marked difference in the freezing point between the upper and lower surfaces of the ice. Close to the upper surface, the ice is almost free of salt so that the freezing point there is close to the fresh-water freezing point θ_{f0}. At the lower surface, the freezing point is that of salt water which is lower than θ_{f0}. Taking the freezing point at the upper surface of the ice to be equal to the fresh-water freezing point, ice melting may occur at its lower surface due to heat conduction caused by the temperature difference across the ice. The evolution of the ice thickness in this regime is governed by Eq. (9). The evolution of θ_i and θ_s are governed by Eqs. (5) and (7). To put it differently, the ice melting occurs at its lower surface, whereas the heat received from the atmosphere raises the heat content of the ice layer.

3 Implementation into GME

The ice model developed in section 2 is implemented into the global NWP system GME of DWD. This first version adopted for operational use is a simplified version of the proposed model. The snow layer over the ice is not considered, the heat flux from water to ice is neglected, and the volumetric character of the solar radiation heating is ignored. Then, the model equations are simplified to give

$$\frac{dH_i}{dt} = -\Phi_i'(0)\frac{\kappa_i}{\rho_i L_f}\frac{\theta_i - \theta_f}{H_i}, \tag{12}$$

$$C_{*i}H_i\frac{d\theta_i}{dt} = -\frac{1}{\rho_i c_i}(Q_a + I_a) - \Phi_i'(0)\frac{\kappa_i}{\rho_i c_i}\frac{\theta_i - \theta_f}{H_i}\left[1 + (1 - C_{*i})R_{\theta i}\right], \tag{13}$$

and

$$\left[1 + (1 - C_{*i})R_{\theta i}\right]\frac{dH_i}{dt} = \frac{1}{\rho_i L_f}(Q_a + I_a), \tag{14}$$

$$\theta_i = \theta_{f0}, \tag{15}$$

where $(1 - C_{*i})R_{\theta i}$ is small as compared to one and can safely be neglected. Equations (14) and (15) should be used when the surface temperature $\theta_s = \theta_i$ has reached the fresh-water freezing point, $\theta_i = \theta_{f0}$, and the heat flows from the atmosphere towards the ice, i.e. $Q_a + I_a < 0$. Otherwise, Eqs. (12) and (13) should be used.

The ice model is currently set up as follows. The simplest linear temperature profile within the ice is used, where $\Phi_i'(0) = 1$ and $C_{*i} = 1/2$. A model of ice growth based on a linear temperature distribution was proposed by Stefan as early as 1891. A slightly more sophisticated approximation for the temperature-profile shape function is developed in Appendix A. The salt-water freezing point is set to a constant value of $\theta_f = 271.45$ K. The ice albedo with respect to solar radiation is computed from

$$\alpha = \alpha_{max} - (\alpha_{max} - \alpha_{min}) \exp\left[-C_\alpha(\theta_{f0} - \theta_i)/\theta_{f0}\right], \tag{16}$$

where $\alpha_{max} = 0.65$ and $\alpha_{min} = 0.40$ are maximum and minimum values of the ice albedo, and $C_\alpha = 95.6$ is a fitting coefficient. Equation (16) is meant to implicitly account (in a crude way) for the seasonal changes of α. During the summer, when the ice surface temperature is close to the fresh-water freezing point, a decrease of the area-averaged albedo occurs due to the presence of meltwater ponds and leads (see e.g. Ebert and Curry 1993). A minimum value of $\alpha_{min} = 0.40$ is close to the estimates of the wavelength-intergrated albedo reported by Ebert and Curry (1993) and Perovich et al. (2002). This value is typical of the summer months in the Arctic. As regards the horizontal distribution of the ice cover, the ice model is obedient to the GME data assimilation scheme. If a GME grid box has been set ice-free during the initialisation, no ice is created over the forecast period. If observational data indicate open water conditions for a given grid box, residual ice from the model forecast is removed and the water surface temperature is set to the observed value. At present, no fractional ice cover is considered. The GME grid box is treated as ice-covered once the assimilation scheme has detected an ice fraction greater than 0.5. The newly formed ice has the thickness of 0.5 m. Prognostic ice thickness is limited by a maximum value of 3 m.

4 Numerical Experiments

The new ice model implemented into GME is tested through numerical experiments including data assimilation. The GME output is compared with available empirical data, with the output from the ECMWF IFS, and with the output from GME using an old ice model. The "old ice model" is actually a parameterization rule used operationally in GME until April 2004. It simply sets the ice surface temperature to a climatologically mean value and keeps it constant over the forecast period once the ice fraction over 0.5 is detected during the initialisation. The ECMWF ice model forecasts the ice surface temperature by solving a finite-difference analogue of the one-dimensional heat transfer equation for the ice slab of fixed depth (IFS Documentation Cycle 25r1 2004).

Figure 1 shows the area-mean ice surface temperature in the Arctic. Results from both GME with the new ice model and from ECMWF IFS are in marked contrast to the results from GME with the old ice model. This is not surprising, however, considering that the air-ice interaction is basically lacking in the old GME ice model. The curves computed by GME with the new ice model and by ECMWF IFS show a very similar behaviour as regards the phase of changes of the ice surface temperature. In December 2003 – February 2004, the ice surface in GME appears to be, on the average, 4 K colder than in the ECMWF IFS. This difference is likely to result from different states of the atmosphere in GME and in ECMWF IFS, not from details of the ice models used. Results from GME test runs (not shown) indicate only marginal changes in the ice surface temperature in response to varying disposable parameters of the new GME ice model (e.g. the temperature-profile shape factor), whereas a different radiation input may account for the ice-surface temperature difference of order ten degrees or more. During summer, the ice albedo with respect to solar radiation proves to be vital to the radiation input. During winter, the radiation input is chiefly governed by the cloud cover and the cloud-radiation interactions (GME uses the radiation scheme developed by Ritter and Geleyn 1992). That such is the case is suggested by the analysis of cloud cover in the Artic. Both the low-level cloud cover and the total cloud cover (not shown) in GME are noticeably lower than in the ECMWF IFS. This is indicative of a lower downward flux of long-wave atmospheric radiation in GME than in the ECMWF IFS. As a consequence a lower ice surface temperature is required to maintain the surface energy budget.

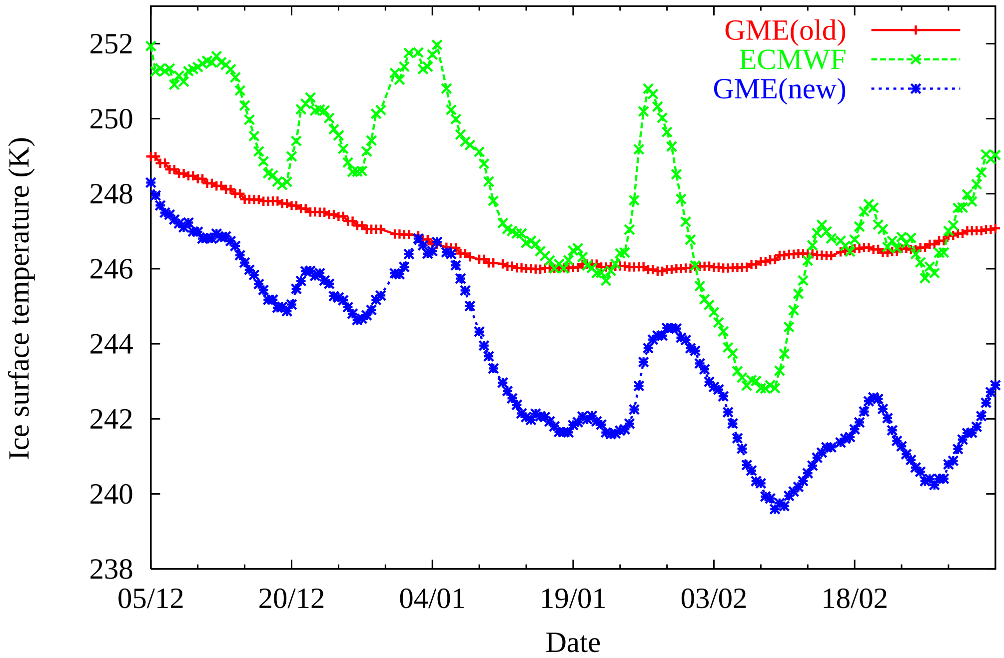

Figure 1: The ice surface temperature in the Artic over the period from 5.12.2003 to 3.3.2004. Blue curve shows the GME analysis using the new ice model, green curve shows the ECMWF analysis, and red curve shows the GME analysis using the old ice model. The curves are computed by means of averaging over all sea ice points north of 65 N latitude, using the GME ice-water mask.

Figure 2 shows the area-mean ice surface temperature in the Antarctic. Again, the old GME climatology is substantially different from both GME and ECMWF IFS forecasts. The two forecasts agree closely, except in the middle of December 2003 when the ice surface is about 1 K warmer in GME than in ECMWF IFS. Notice that both GME and ECMWF IFS predict a day-night ice surface temperature difference of order 0.5 K during austral summer. Obviously, there are no diurnal variations of the ice surface temperature in the winter hemisphere (Fig. 1).

Figure 3 shows the two-metre temperature in the Arctic, as computed by GME with the new ice model and with the old ice model, versus observations. The two simulations show different spatial temperature structure. The simulation with the new ice model shows a better agreement with data as compared to the simulation with the old ice model. The results with the new model reveal a somewhat lower bias of -4.5 K versus -5.9 K for the simulation with the old model, and a lower root-mean-square error, 3.6 K versus 7.2 K, respectively. In spite of sparsity and possible uncertainties of available observational data, this counts in favour of the new ice model. Still the ice surface in GME is a bit too cold. The ice thickness in the Arctic computed with the new GME ice model is illustrated in Fig. 4. The ice thickness distribution looks reasonable. This is difficult to verify quantitatively, however, for lack of observational data.

Figure 5 shows verification scores for GME with the two versions of the ice model. The impact of the new ice model on the quality of the global forecast is marginal. By and large this result can be taken as positive, considering that the new ice model introduces an extra degree of

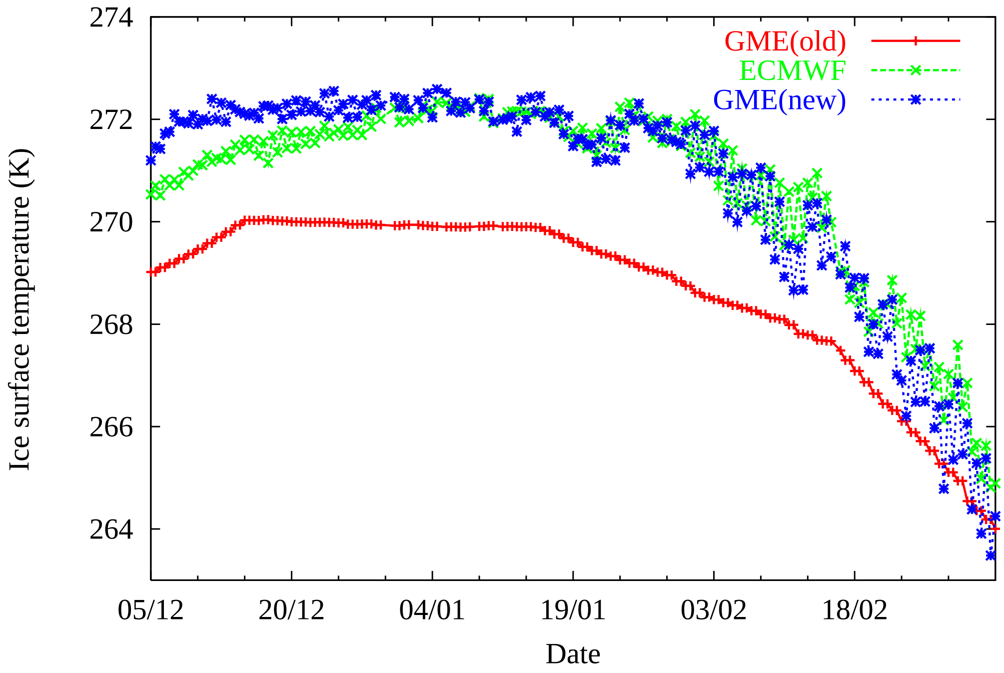

Figure 2: Same as in Fig. 1 for the Antarctic south of 65 S latitude.

freedom into GME.

5 Conclusions

A thermodynamic ice model is developed and implemented into the global NWP system GME of the German Weather Service. A distinguishing feature of the proposed model is the treatment of the heat transfer through the ice. Most currently used ice models carry the heat transfer equation that is solved on a finite difference grid where the number of grid points and the grid spacing differ with the application. We use the integral, or bulk, approach. It is based on a parametric representation (assumed shape) of the evolving temperature profile within the ice and on the integral heat budget of the ice slab. The proposed ice model solves two ordinary differential equations for the two time-dependent quantities, the ice surface temperature and the ice thickness. As regards the horizontal distribution of the ice cover, it is governed by the GME data assimilation scheme.

Results from numerical experiments show a satisfactory performance of the new ice model. Neither the ice surface temperature nor the ice thickness are overly sensitive to the details of the ice model itself. This is a very encouraging result as it justifies the use of a simplified ice model in NWP systems. The use of an integral approach instead of a finite-difference approach to describe the heat transfer through the ice allows to save computational resources without any detectable loss in accuracy of the results. The ice surface temperature proves to be sensitive to the cloud cover, particularly during winter. During summer, also the ice albedo with respect to solar radiation appears to play a major part in forecasting the ice surface temperature. In the present operational configuration of GME, an empirical formulation is used, where the ice albedo depends on the ice surface temperature. That formulation is meant to implicitly account, in a rather crude way, for the seasonal changes of the ice albedo. Further efforts should go into the development of a refined formulation for the ice albedo. A snow layer over the ice may also need to be considered. In section 2, provision is made to account for the snow layer using the bulk model framework.

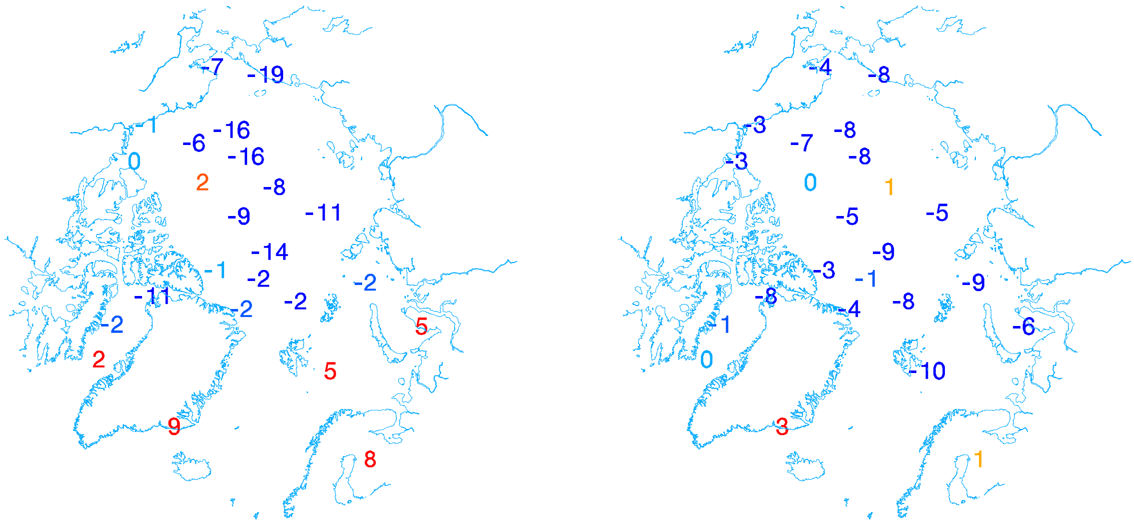

Figure 3: The two-metre temperature in the Arctic at 12 UTC on 1.1.2004: left panel – GME analysis using the old ice model, right panel – GME analysis using the new ice model. Numbers show computed minus observed two-metre temperature difference (in K).

Acknowledgements. We thank Michael Buchhold, Thomas Hanisch, Erdmannn Heise, Aurelia Müller and other colleagues at DWD for numerous discussions and helpful suggestions and for their help in implementing and testing the new ice model in GME. The ECMWF forecast products used for comparison are taken from the ECMWF MARS archive. The work was partially supported by the EC Project INTAS-01-2132.

References

Arsenyev, S. A., and A. I. Felzenbaum, 1977: Integral model of the active ocean layer. *Izv. Akad. Nauk SSSR. Fizika Atmosfery i Okeana*, **13**, 1034–1043.

Deardorff, J. W., 1979: Prediction of convective mixed-layer entrainment for realistic capping inversion structure. *J. Atmos. Sci.*, **36**, 424–436.

Ebert, E. E., and J. A. Curry, 1993: An intermediate one-dimensional thermodynamic sea ice model for investigating ice-atmosphere interactions. *J. Geophys. Res.*, **98**, 10,085–10,109.

Fedorovich, E. E., and D. V. Mironov, 1995: A model for shear-free convective boundary layer with parameterized capping inversion structure. *J. Atmos. Sci.*, **52**, 83–95.

Filyushkin, B. N., and Yu. Z. Miropolsky, 1981: Seasonal variability of the upper thermocline and self-similarity of temperature profiles. *Okeanologia*, **21**, 416–424.

IFS Documentation Cycle 25r1, 2004. Available from the web site of ECMWF, `http://www.ecmwf.int/research`.

Kamenkovich, V. M., and B. V. Kharkov, 1975: On the seasonal variation of the thermal structure of the upper layer in the ocean. *Okeanologia*, **15**, 978–987.

Kitaigorodskii, S. A., and Yu. Z. Miropolsky, 1970: On the theory of the open ocean active layer. *Izv. Akad. Nauk SSSR. Fizika Atmosfery i Okeana*, **6**, 178–188.

Launiainen, J., and B. Cheng, 1998: Modelling of ice thermodynamics in natural water bodies. *Cold. Reg. Sci. Technol.*, **27**, 153–178.

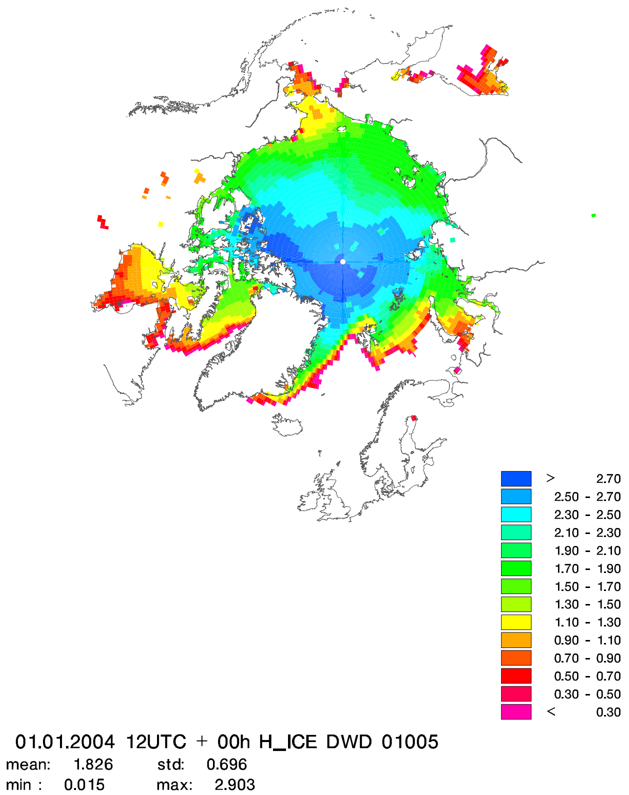

Figure 4: The ice thickness H_i in the Arctic at 12 UTC on 1.1.2004 computed with the new ice model.

Leppäranta, M., 1993: A review of analytical models of sea-ice growth. *Atmosphere-Ocean*, **31**, 123–138.

Majewski, D., D. Liermann, P. Prohl, B. Ritter, M. Buchhold, T. Hanisch, G. Paul, W. Wergen, and J. Baumgardner, 2002: Icosahedral-hexagonal gridpoint model GME: description and high-resolution tests. *Mon. Weather Rev.*, **130**, 319–338.

Mironov, D., 2004: Parameterization of lakes in numerical weather prediction. Part 1: Description of a lake model. In preparation (manuscript is available from the author).

Mironov, D. V., S. D. Golosov, S. S. Zilitinkevich, K. D. Kreiman, and A. Yu. Terzhevik, 1991: Seasonal changes of temperature and mixing conditions in a lake. *Modelling Air-Lake Interaction. Physical Background*, S. S. Zilitinkevich, Ed., Springer-Verlag, Berlin, etc., 74–90.

Perovich, D. K., T. C. Grenfell, B. Light, and P. V. Hobbs, 2002: Seasonal evolution of the albedo of multiyear Arctic sea ice. *J. Geophys. Res.*, **107**(C10), 8044, doi:10.1029/2000JC000438.

Ritter, B., and J.-F. Geleyn, 1992: A comprehensive radiation scheme for numerical weather prediction models with potential applications in climate simulations. *Mon. Weather Rev.*, **120**, 303–325.

Semtner, A. J., 1976: A model for the thermodynamic growth of sea ice in numerical investigations of climate. *J. Phys. Oceanogr.*, **6**, 379–389.

Stefan, J., 1891: Ueber die Theorie der Eisbildung, insbesondere über die Eisbildung im Polarmeere. *Ann. Phys.*, **42**, 269–286.

Zilitinkevich, S. S., 1991: *Turbulent Penetrative Convection.* Avebury Technical, Aldershot, 179 pp.

Zilitinkevich, S. S., E. E. Fedorovich, and D. V. Mironov, 1992: Turbulent heat transfer in stratified geophysical flows. *Recent Advances in Heat Transfer*, B. Sundén and A. Žukauskas, Eds., Elsevier Science Publisher B. V., Amsterdam, etc., 1123–1139.

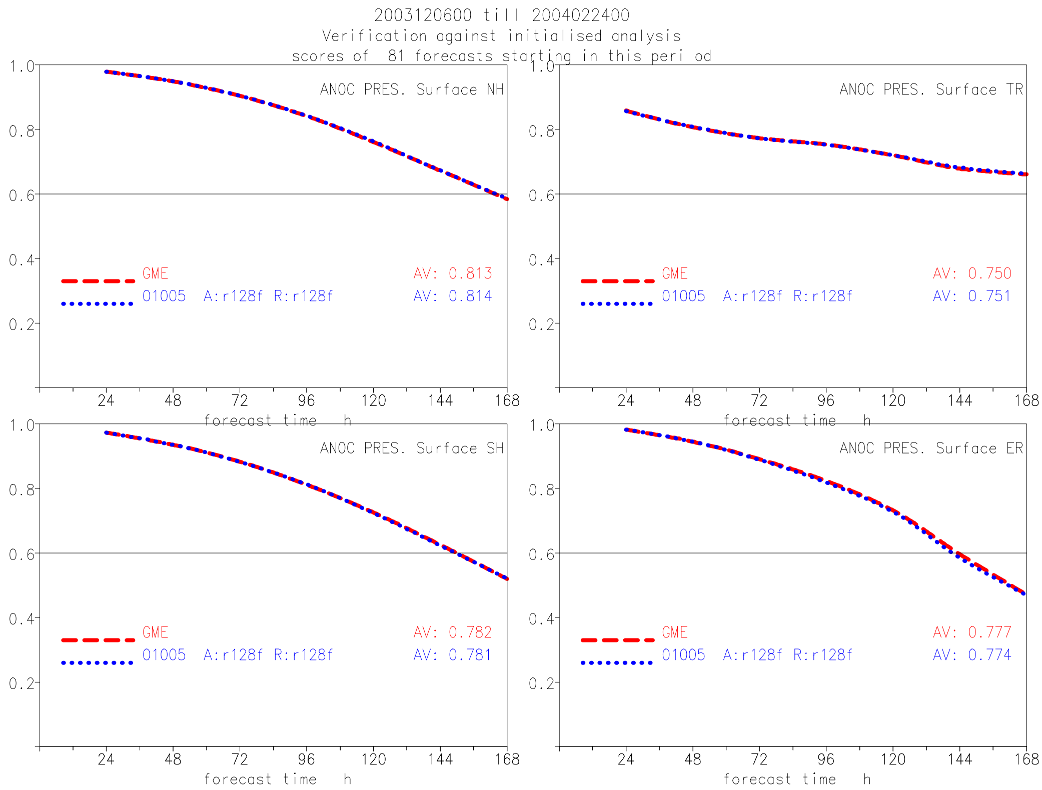

Figure 5: Verification scores for GME using the new ice model, blue curves, and the old ice model, red curves. The scores are for mean sea level pressure for northern hemisphere (upper left), tropics (upper right), southern hemisphere (lower left) and Europe (lower right). They are based on the GME analysis over the period from 6.12.2003 to 24.02.2004.

Appendix A. The Temperature-Profile Shape Function

Although a linear profile is a good approximation for thin ice, it is likely to result in a too thick ice in cold regions, where the ice growth takes place over most of the year, and in a too high thermal inertia of thick ice. A slightly more sophisticated approximation is developed by assuming that the ice thickness is limited by a certain maximum value H_{im} and that the rate of ice grows approaches zero as H_i approaches H_{im}. We propose

$$\Phi_i'(0) = 1 - \frac{H_i}{H_{im}}, \qquad C_{*i} = \frac{1}{2} - \frac{1}{12}(1+\Phi_*)\frac{H_i}{H_{im}}, \tag{A.1}$$

where Φ_* is a dimensionless constant. The physical meaning of the above expressions can be elucidated as follows. The first member of Eq. (A.1) ensures that the ice growth is quenched as the ice thickness approaches its maximum value. The second member of Eq. (A.1) suggests that the shape factor decreases with increasing ice thickness. A smaller C_{*i} means a smaller relative thermal inertia of the ice layer of thickness H_i [the absolute thermal inertia is measured by the term $C_{*i}H_i$ that multiplies $d\theta_i/dt$ on the l.h.s. of Eq. (13)]. This is plausible as it is mostly the upper part of thick ice, not the entire ice layer, that effectively responds to external forcing. The ice model has only two tuning parameters. A reasonable estimate of the maximum ice thickness is $H_{im} = 3$ m. This value is typical of the central Artic in winter. The allowable values of Φ_* lie in the range between -1 and 5. $\Phi_* > 5$ yields an unphysical negative value of C_{*i} as the ice thickness approaches H_{im}. $\Phi_* < -1$ gives C_{*i} that increases with increasing H_i. There is no formal proof that this may not occur, but it is very unlikely. A reasonable estimate is $\Phi_* = 2$. With this estimate C_{*i} is halved as H_i increases from 0 to H_{im}. Notice that the linear temperature profile is recovered as $H_i/H_{im} \ll 1$, i.e. when the ice is thin.

One further comment is in order regarding the expressions (A.1). These expressions may be viewed as corresponding to the third-order polynomial approximation of the temperature-profile shape function $\Phi_i(\zeta_i)$. The third-order polynomial is the simplest approximation that satisfies a minimum set of constraints. The polynomial coefficients are determined as follows. First, the boundary conditions $\Phi_i(0) = 0$ and $\Phi_i(1) = 1$ are satisfied that simply follow from the definition of Φ_i and ζ_i. Second, the conditions (A.1) are satisfied, where the shape factor is defined through the first member of (6). The dependence of $\Phi_i'(0)$ and C_{*i} on H_i/H_{im} is chosen so that to ensure the desired behaviour of the ice growth rate and of the thermal inertia of the ice layer. This approach, that could be called "verifiable empiricism", heavily relies on empirical data. However, it still incorporates much of the essential physics and offers a good compromise between physical realism and computational economy. The third-order polynomial approximation of the temperature profile shape function is illustrated in Fig. 6. As seen from the figure, the temperature profile is almost linear when the ice is thin, $H_i \ll H_{im}$, and is given by the left solid curve as the ice thickness H_i approaches its maximum value H_{im}.

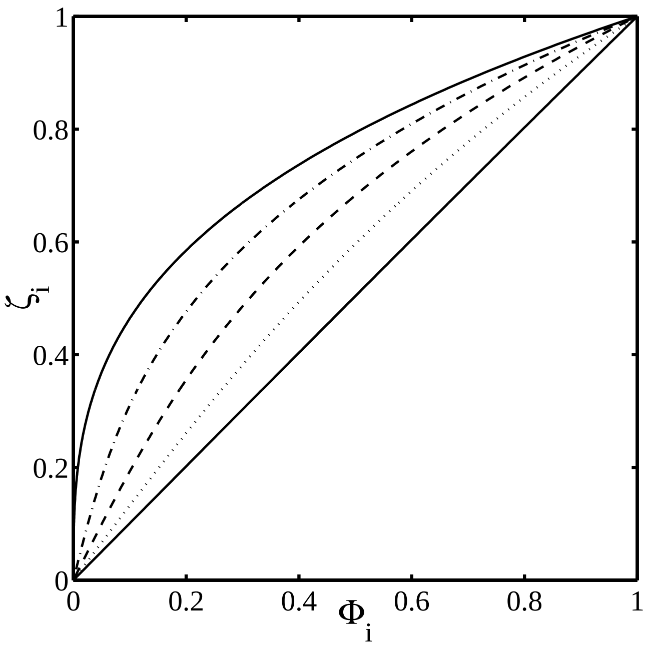

Figure 6: The approximation of the temperature profile shape function $\Phi_i(\zeta_i)$ with the third-order polynomial whose coefficients satisfy Eq. (A.1). The curves are computed with $\Phi_* = 2$ and (from right to left) $H_i/H_{im} = 0.01$, $H_i/H_{im} = 0.25$, $H_i/H_{im} = 0.5$, $H_i/H_{im} = 0.75$ and $H_i/H_{im} = 1.0$.